Journal of Power Sources 272 (2014) 203–210

Contents lists available at ScienceDirect

Journal of Power Sources

journal homepage: www.elsevier.com/locate/jpowsour

Petal-shaped poly(3,4-ethylenedioxythiophene)/sodium dodecyl sulfate-graphene oxide intercalation composites for high-performance electrochemical energy storage

Haihan Zhou*, Gaoyi Han*, Dongying Fu, Yunzhen Chang, Yaoming Xiao, Hua-Jin Zhai

Institute of Molecular Science, Key Laboratory of Chemical Biology and Molecular Engineering of Education Ministry, Shanxi University, Taiyuan 030006, China

HIGHLIGHTS

- PEDOT/SDS-GO intercalation composites are prepared with a facile electrochemical method.
- The intercalation composites possess a unique petal-shaped morphology.
- Incorporation of GO into the composites effectively boosts the capacitive performance.
- The composites reveal large areal capacitance and excellent cycle stability.

ARTICLE INFO

Article history:
Received 13 June 2014
Received in revised form
15 July 2014
Accepted 19 August 2014
Available online 29 August 2014

Keywords:
Electrochemical capacitors
Poly(3,4-ethylenedioxythiophene)
Graphene oxide
Anionic surfactants
Areal capacitance

ABSTRACT

A facile and one-step electrochemical codeposition method is introduced for incorporating graphene oxide (GO) into poly(3,4-ethylenedioxythiophene) (PEDOT) films in the presence of sodium dodecyl sulfate (SDS). The as-prepared PEDOT/SDS-GO composites are characterized using scanning electron microscope, transmission electron microscopy, Fourier transform infrared spectroscopy, and X-ray diffraction. The results show that PEDOT/SDS-GO composites possessing a unique petal-shaped morphology have been prepared successfully and exhibit an intercalated microstructure. With the purpose of electrochemical energy storage, the properties of electrochemical capacitance for composites have also been investigated with cyclic voltammetry, galvanostatic charge/discharge measurements, and electrochemical impedance spectroscopy tests. The electrochemical test results manifest the PEDOT/SDS-GO composites have superior capacitive behaviors and cyclic stability, and a high areal capacitance of 79.6 mF cm^{-2} is achieved at 10 mV s^{-1} cyclic voltammetry scan. Furthermore, the PEDOT/SDS-GO composites exhibit more superior capacitive performance than that of PEDOT/SDS, indicating the incorporation of GO into the composites effectively boosts the capacitive performance of PEDOT-based supercapacitor electrodes. We consider that this research further extends the application of GO and the composites prepared can be developed as the candidate for the fabrication of low-cost, high-performance supercapacitors for energy storage.

1. Introduction

Due to the high power density and cyclability relative to secondary batteries, electrochemical capacitors (also called supercapacitors) have been extensively studied nowadays, and they are expected to be applied in some fields that require electrical energy at high power levels in relatively short pulses, such as hybrid electric vehicles, portable electronics, digital communications, and so on [1–6]. Recent research efforts have been focused on improving the energy density of supercapacitors by developing new electrode materials [7–10].

On the basis of charge storage mechanism, supercapacitors can be divided into electrical double-layer capacitors (EDLCs) and redox supercapacitors [11,12]. The main electrode materials used for EDLCs are based on carbon materials, such as activated carbon, carbon nanotubes, and graphene, etc., and the energy storage in EDLCs is derived from the charging of the electrical double layer at the electrode-electrolyte interface; while the electroactive materials with several redox states or structures for the redox supercapacitors,

* Corresponding authors. Tel.: +86 351 7010699; fax: +86 351 7016358.
E-mail addresses: hhzhou@sxu.edu.cn (H. Zhou), han_gaoyis@sxu.edu.cn (G. Han).

http://dx.doi.org/10.1016/j.jpowsour.2014.08.073
0378-7753/

such as transition-metal oxides (e.g., oxides of ruthenium, nickel, cobalt, indium) and conducting polymers (CPs), and the energy of redox supercapacitor is stored by a fast and reversible faradaic redox reaction in addition to the double-layer charge [13,14]. Commonly, EDLCs is due to the electrosorption of ions on porous carbon electrodes, consequently limited energy density, pseudo-capacitors provide higher energy densities but usually suffer from shorter cyclic lifetimes [15,16]. Based on these, considerable attention has been devoted to exploring hybrid materials combining the advantages of EDLCs and redox supercapacitors to obtain high-performance capacitive electrode materials [17–21].

Currently, many researchers have studied poly(3,4-ethylenedioxythiophene) (PEDOT) as the electrode material for supercapacitors, because the PEDOT exhibits not only a high conductivity but also an unusual stability in the oxidized state compared to other types of conducting polymers (CPs) [22]. Graphene oxide (GO), with a low fabrication cost and an environmentally friendly nature, can easily be synthesized from natural graphite and form stable dispersions in water, and the good dispersibility is ascribed to the GO flakes have a negative surface, which is derived from the charge highly oxidized structure with a large number of oxygen containing functional groups (alkoxy, epoxy, carbonyl, and carboxyl groups) [23,24]. Some studies have been devoted to developing the composites of CPs and GO nanosheets to achieve a multilayered configuration with high specific capacitance and low electronic resistance for supercapacitor electrode applications. However, these materials were usually prepared through complicated multiple-step procedures or using the chemical oxidative polymerization [25–27]. In comparison to chemical oxidative polymerization, electrochemical polymerization show the advantages that the films can be deposited directly on the electrode substrates, and the film thickness can easily be controlled and the films are free from impurities (e.g. the oxidant and its reaction products). Fortunately, the anionic character of GO makes it possible to act as dopant during electrochemical polymerization of conducting polymers to form CPs/GO composite films deposited on a variety of electrode substrates. Currently, the one-step electrochemical codeposition of CPs and GO has been reported [28,29], in our previous study, the GO nanosheets were incorporated into the polypyrrole (PPy) matrix to form the PPy/GO composite electrodes possessing large areal capacitance using a facile one-step electrochemical codeposition method [30]. The study by Österholm et al. [31] also showed the one-step electrochemical deposition of PEDOT–GO and PPy–GO composite films from aqueous GO dispersions without any additional dopants, and the CV tests indicated that the higher charge capacity for PPy–GO than for PPy–Cl as a result of the incorporation of GO sheets. But unlike the PPy–GO, PEDOT–GO showed redox current and charge values were significantly lower compared to those of PEDOT-poly(styrene sulfonate), and the SEM images suggested that incorporation of GO resulted in a smoother surface morphology with a lower effective surface area, consequently, a lower redox current. Likewise, our preliminary investigation also indicated the direct incorporation of GO into the PEDOT without any additional dopants was unfavourable for improving the capacitive performance of PEDOT-based electrodes. However, we found using the anionic surfactants such as sodium dodecyl sulfate (SDS) micellar aqueous medium can improve the electrosynthesis and physicochemical properties of PEDOT through the literature survey [32]. Therefore, adding the SDS into the polymerization system of PEDOT has the potential to highlight the advantage of incorporating the GO nanosheets into PEDOT matrix.

Herein, PEDOT/SDS-GO composites have been synthesized by a facile electrochemical codeposition method in aqueous media containing GO dispersions and EDOT monomer, in which SDS serves as supporting electrolyte as well as counter-ions and dispersant to promote the dispersion of GO. As the comparison, PEDOT/SDS has also been prepared under the polymerization system without GO dispersions using the same electrochemical procedure. The compositions and morphology as well as the structures of the composites were studied using scanning electron microscope (SEM), transmission electron microscopy (TEM), Fourier transform infrared spectroscopy (FT-IR), and X-ray diffraction (XRD). The electrochemical behaviors of PEDOT/SDS-GO and PEDOT/SDS were investigated and compared using cyclic voltammetry (CV), galvanostatic charge/discharge (GCD) measurements, and electrochemical impedance spectroscopy (EIS). The composite electrode materials are expected to greatly improve the performances of the PEDOT-based supercapacitors and lead to a higher energy and power capability for various applications.

2. Experimental

2.1. Materials

3,4-Ethylenedioxythiophene (EDOT, Ourchem®, 99%) was purchased from Sinopharm Chemical Reagent Co. Ltd (Shanghai, China), sodium dodecyl sulfate (SDS, AR) was obtained from Tianjin Fangzheng Reagent Plant. Natural graphite powder (325 mesh) was purchased from Tianjin Guangfu Research Institute. FTO conducting glasses were obtained from Dalian Heptachroma SolarTech (DHS-FTO22-8-02, 8 $\Omega\ \square^{-1}$), as shown in Fig. 1a, 1 cm × 1 cm conductive areas were exposed as the substrate for electrochemical deposition. Prior to use, the glasses were ultrasonically cleaned in acetone and deionized water successively.

2.2. Electrode preparation

As shown in Fig. 1a, the supercapacitor electrodes were fabricated by electrochemically codepositing PEDOT/SDS-GO intercalation composite films onto the FTO conductive glasses. Before deposition, GO was prepared by oxidizing the natural graphite powder and subsequent exfoliation by ultrasonication according to the method reported in literature [33,34]. The obtained GO aqueous dispersion was treated with freeze drying and preserved at the room temperature. For the procedure of deposition, an aqueous solution containing 0.01 M EDOT monomer, 2 mg mL^{-1} GO, and 0.01 M SDS was dispersed under ultrasonication for about 15 min to form a metastable homogenous colloidal solution, in which SDS serves as supporting electrolyte as well as counter-ions and dispersant to promote the dispersion of GO. Subsequently, PEDOT/SDS-GO films were electrodeposited onto the FTO conducting glasses with a galvanostatic mode, in which a current of 1.0 mA cm^{-2} was applied for 30 min. After that, the composite films-deposited glasses were washed with adequate deionized water to remove the unreacted substance. During the deposition, the cleaned FTO conducting glasses were fixed in a two-electrode cell with a large-area Pt sheet acting as the counter electrode and pseudo-reference electrode. As the comparison, PEDOT/SDS electrodes were deposited from an aqueous solution containing 0.01 M EDOT monomer and 0.1 M SDS, and the procedure of deposition is identical with that of the PEDOT/SDS-GO electrodes. The mass of PEDOT/SDS and PEDOT/SDS-GO films was measured by weighing the changes of FTO conducting glasses before and after depositing films. For FT-IR test, pure PEDOT films were deposited from solutions containing 0.01 M EDOT monomer and 0.1 M KCl with the same procedure.

2.3. Morphology

The surface morphology of the PEDOT/SDS-GO and PEDOT/SDS films was observed using a field emission scanning electron microscope (JSM-6701F, JEOL) operated with a voltage of 10.0 kV. The

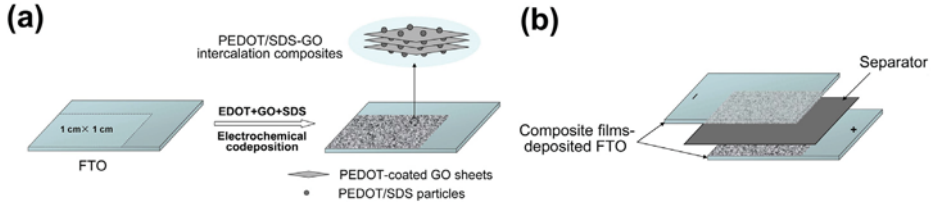

Fig. 1. (a) Schematic representation for the electrochemical codeposition of PEDOT/SDS-GO intercalation composites; (b) The supercapacitor cells consisted of two pieces of symmetric composite films-deposited FTO conducting glasses for electrochemical measurements.

microstructures of GO, PEDOT/SDS, and PEDOT/SDS-GO were examined with a high resolution transmission electron microscopy (JEM-2100, JEOL) operating at 200 kV.

2.4. Composition and structural characterization

The test films were scraped from the surface of films-deposited FTO conducting glasses for the thickness, FT-IR, and XRD tests. FT-IR spectra were obtained with a Bruker Tensor 27 FT-IR spectrometer, and all samples were prepared by potassium bromide tabletting. The X-ray diffraction (XRD) patterns of the samples were recorded on a Bruker D8 Advance X-ray diffraction meter with Cu Kα radiation and graphite monochromator, at the scan speed of 5° min^{-1} with a step size of 0.02°.

2.5. Electrochemical measurements

For the electrochemical measurements, the capacitor cells (Fig. 1b) were assembled by using two pieces of composite films-deposited FTO conducting glasses (one oxidized and one reduced) as the two electrodes, a filter paper soaked with 1.0 M KCl electrolyte served as the separator, the conducting glass itself was used as the current collector. All the electrochemical measurements were carried out on an electrochemical workstation (CHI 660B, Chenhua, China) using two-electrode system. The CV measurements were performed between potentials of −0.5 to 0.5 V, and the scan rates ranged from 10 to 200 mV s^{-1}. The GCD tests were performed at varying current density with the cutoff voltage of −0.5 and 0.5 V. The EIS were measured using 5 mV (rms) AC sinusoid signal and at a frequency range from 100 k to 0.01 Hz at the open circuit potential. During the aforementioned electrochemical tests, the assembled cells were wrapped with a preservative film to prevent the volatilization of electrolyte.

3. Results and discussion

3.1. Morphology

The surface morphology is an important parameter if the films are to be used as electrode materials in electrochemical devices. In this research, the thickness of PEDOT/SDS and PEDOT/SDS-GO films deposited is 16 and 12 μm, respectively, and their mass is 2.4 and 1.4 mg, respectively. Fig. 2 shows the SEM images of PEDOT/SDS and PEDOT/SDS-GO composite films. The image of PEDOT/SDS displays a leaves-like morphology, but these leaves cumulate densely, which may be unfavourable for the access of electrolyte. However, a significant change in the morphology is observed when the films are polymerized in the presence of GO, the PEDOT/SDS-GO films exhibit a petal-shaped morphology, and these cumulate petals construct a loose and porous microstructure, which is positive to the ions and electrons transport. In addition, we can observe the curly sheets from the inset of PEDOT/SDS-GO image, it is in accord with the microstructure of GO, indicating the sheet-like GO is dominant in the morphology of composite films, namely, GO act as counter-ions and substrate, PEDOT and PEDOT/SDS coat on the surface and intercalate between the GO sheets to form the intercalation composites. This will be further testified in the following section. It is well known that electrochemical performance of an electrode is strongly influenced by its microstructure and the active surface area accessible to the electrolyte. The special petal-shaped microstructure of PEDOT/SDS-GO composites induced by incorporating the GO could facilitate the increase of electroactive area and access of electrolyte.

In order to further observe the composite morphology of PEDOT/SDS-GO composites, TEM characterization was made and the images are shown in Fig. 3. As expected, the GO shows the

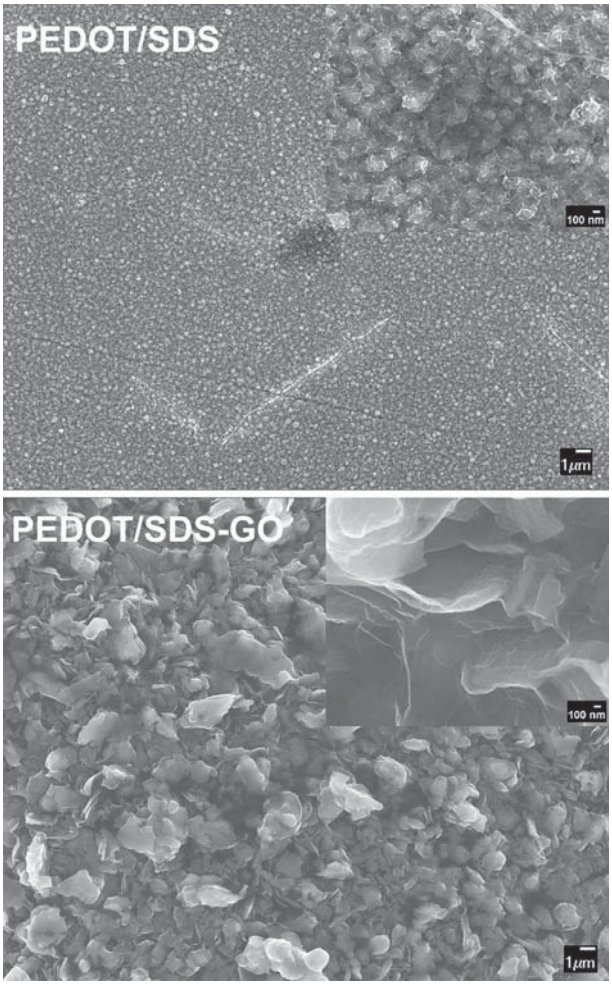

Fig. 2. SEM images of PEDOT/SDS and PEDOT/SDS-GO composite films. The insets in the upper right are the SEM images in high magnification. The thickness of PEDOT/SDS and PEDOT/SDS-GO composite films is 16 and 12 μm, respectively.

sheet-like morphology with smooth and slightly curly edge, meanwhile, the nanosheets present a large surface area. However, PEDOT/SDS shows the morphology of irregular block aggregates. Compared to the GO and PEDOT/SDS, PEDOT/SDS-GO composites display the overlapped structure with multilayer GO nanosheets and the wrinkle of GO disappeared, which accords with the previous report that the wrinkle of GO would decrease with the increase of layers for GO sheets [35]. A careful inspection of the microstructure of PEDOT/SDS-GO composites suggests that PEDOT distribute both on the surface and around the edge of the GO nanosheets (red arrows), and the PEDOT/SDS particles are decorated dispersedly on the surface and intercalate between the GO sheets (blue arrows). TEM images reveal that the GO acted as the counter-ion and substrate during the electrochemical polymerization, PEDOT and PEDOT/SDS coated on the two-dimensional GO surface and filled between the GO nanosheets to form the petal-shaped intercalation composites. This intercalated composite microstructure will facilitate increasing the electroactive area and can combine the advantages of EDLCs and redox supercapacitors originated in carbon materials and CPs.

3.2. Compositions and structures

During the electrochemical codeposition, the anionic GO not only served as the counter-ion for polymerization of EDOT but also as the substrate for the adhesion and intercalation of PEDOT/SDS particles. To determine the compositions and structures of the PEDOT/SDS-GO intercalation composites, FT-IR and XRD tests were carried out and the FT-IR spectra of GO, PEDOT, PEDOT/SDS, and PEDOT/SDS-GO are shown in Fig. 4a. In the spectrum of GO, the peak at 1703 cm^{-1} can be attributed to the C═O stretching of carbonyl. The peaks observed at 1413 and 1235 cm^{-1} represent the O–H deformation and C–OH stretching vibration, in addition, the peak at 1055 cm^{-1} is the characteristic peak of epoxide group [36]. For the pure PEDOT spectrum, the vibrations around 1350 and 1518 cm^{-1} are attributed to the quinoid structure and stretching modes of C–C and C═C in the thiophene ring, respectively [37]. Vibrations at 1203, 1144, 1089, and 1058 cm^{-1} originate from stretching of the C–O–C bond in the ethylenedioxy group [38]. Peak at 926 cm^{-1} is corresponding to the ethylenedioxy ring deformation mode [39], and the vibration modes of the C–S bond in the thiophene ring are seen at 692, 841 and 980 cm^{-1} [38,40]. With the pure PEDOT spectrum as the reference, the FT-IR spectra of both PEDOT/SDS and PEDOT/SDS-GO show the characteristic peaks of PEDOT. The only difference is that the vibration band attributed to C–C stretching in the thiophene ring in PEDOT/SDS and PEDOT/SDS-GO has a redshift from 1350 to 1335 and 1330 cm^{-1} (marked with red). This is related to the electrostatic interaction between the PEDOT cations and the SDS anions as well as the π–π interactions and hydrogen bonding between the GO layers and thiophene rings. It should be noted that GO bands are scarcely detectable in the PEDOT/SDS-GO spectrum, probably because either they are too weak or overlapped with the absorption peak of PEDOT.

The as-prepared composites were further characterized by XRD. As shown in Fig. 4b, XRD pattern of the GO reveals an intense, sharp peak centered at $2\theta = 10.9°$, corresponding to an interplanar spacing (d-spacing) of 0.81 nm of the GO sheets calculated by the Bragg equation. This value is larger than the d-spacing (0.335 nm) of pristine graphite ($2\theta = 26.6°$) as a result of the introduction of oxygenated functional groups [41]. Furthermore, the broad peak at 21.4° indicates that the GO sheets exhibit some aggregations [42]. For the PEDOT pattern, a broad diffraction peak at $2\theta = 26°$ is observed, indicating that the PEDOT is amorphous in nature [43]. In

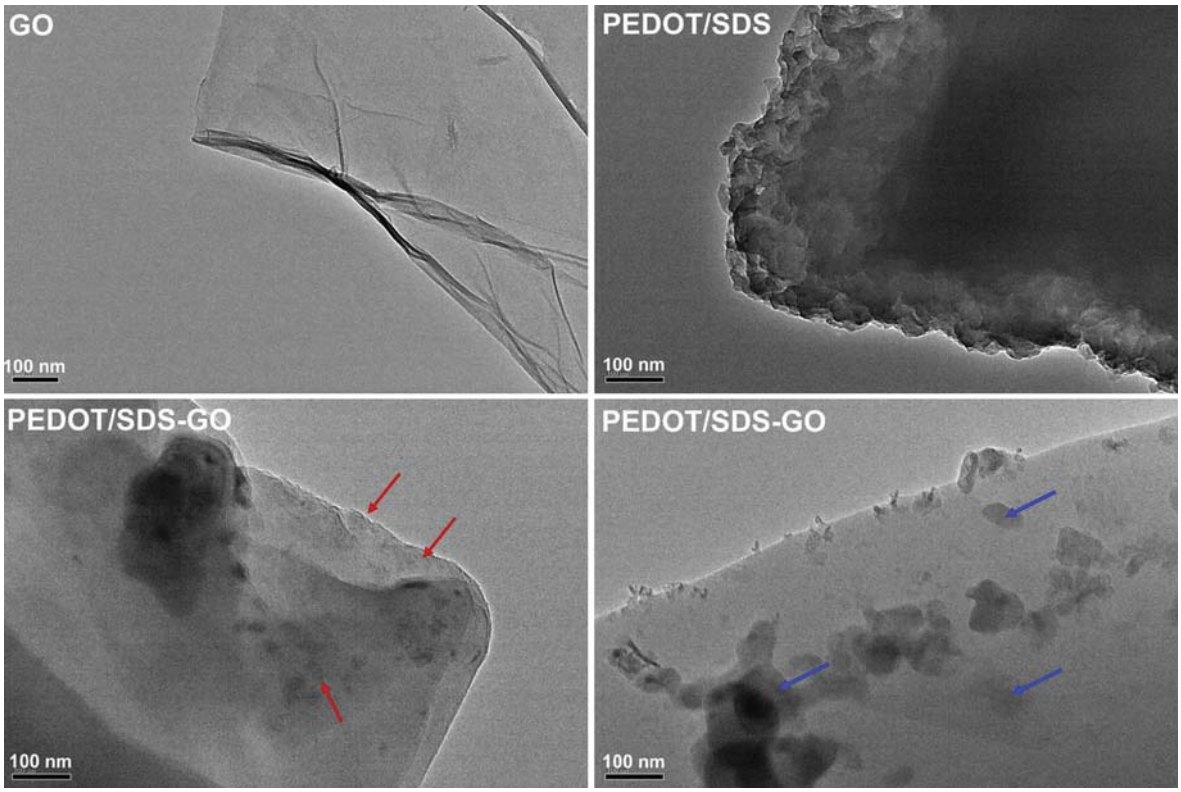

Fig. 3. TEM images of GO, PEDOT/SDS, and PEDOT/SDS-GO composites. For PEDOT/SDS-GO images, red arrows show the PEDOT distribute both on the surface and around the edge of the GO sheets, while blue arrows show the PEDOT/SDS particles are decorated dispersedly on the surface and intercalate between the GO sheets. (For interpretation of the references to color in this figure legend, the reader is referred to the web version of this article.)

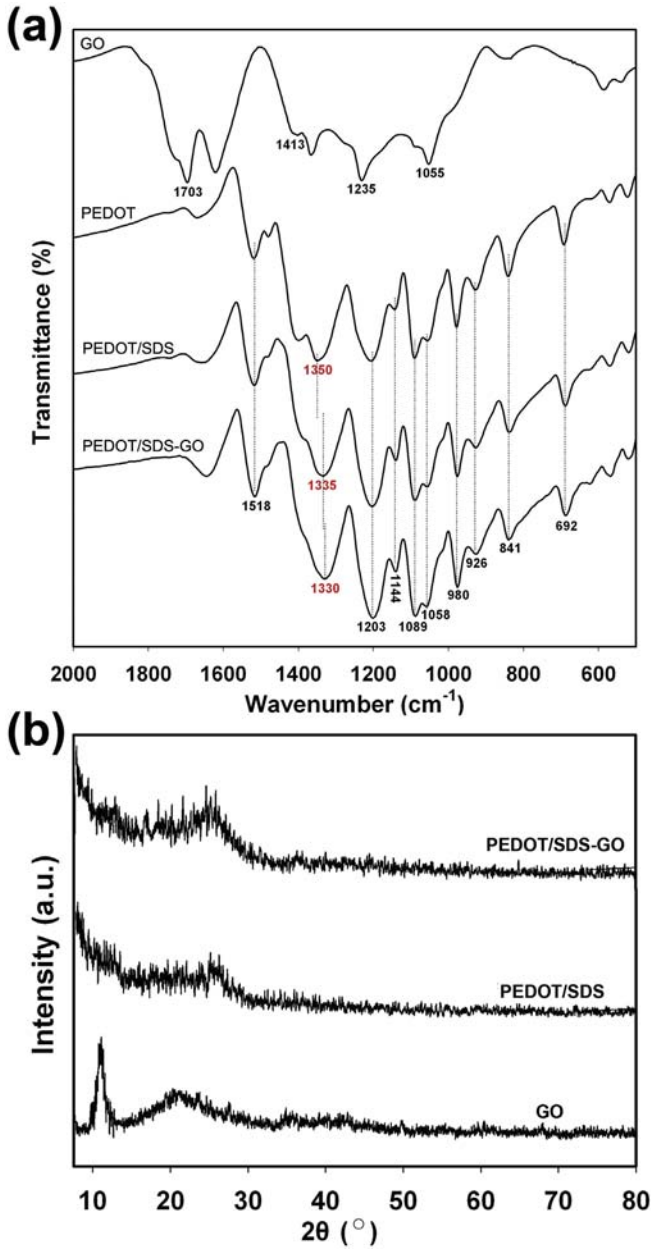

Fig. 4. (a) FT-IR spectra of GO, PEDOT, PEDOT/SDS, and PEDOT/SDS-GO composites; (b) XRD patterns of GO, PEDOT/SDS, and PEDOT/SDS-GO composites.

the case of the PEDOT/SDS-GO composites, only the broad peak situating at 26° attributed to the diffraction peak of PEDOT is shown, additionally, the peak ascribed to GO within composites almost disappears, indicating the PEDOT coatings and the scattered PEDOT/SDS particles between the GO nanosheets increase the d-spacing of the layered GO, which further demonstrate the formation of PEDOT/SDS-GO intercalation composites.

3.3. Electrochemical properties

As an effective tool, CV is commonly to investigate the capacitive behavior of electrode materials. For an ideal capacitor material, it will exhibit several characteristics such as high current, rectangular voltammogram and symmetry in anodic and cathodic directions. In this research, the capacitive behavior was investigated using two-electrode cells, which allow a good estimation of materials performance in electrochemical capacitors [44]. Fig. 5a compares the CV of PEDOT/SDS and PEDOT/SDS-GO electrodes at varying scan rates rang from 10 to 200 mV s^{-1}. It can be seen from the 10 mV s^{-1} plots that the PEDOT/SDS-GO electrodes shows more rectangular-like shape and larger areal CV curve compared with those of the PEDOT/SDS electrodes, which indicate the PEDOT/SDS-GO electrodes exhibit more ideal capacitive behavior. Furthermore, the rectangular-like CV curves with the almost symmetric I-E responses can be also observed at higher scan rates range from 20 to 200 mV s^{-1} and the obvious increase of current with scan rates, demonstrating that the PEDOT/SDS-GO exhibit good capacitive behavior for rapid charge and discharge, and the PEDOT/SDS-GO electrodes still show the larger areal CV curves than those of the PEDOT/SDS electrodes at all scan rates. Aiming for the applications such as small scale electronics and stationary energy storage devices, areal capacitance is a better indicator of the supercapacitor performance than mass specific capacitance [45–47], so this research focuses on the areal capacitance of electrodes. On the basis of the CV curves, the areal capacitance (C_S) value of a single electrode can be calculated according to the following Equation (1):

$$C_S = \left(\int idV\right)/(S \times \Delta V \times v) \quad (1)$$

where C_s is the areal capacitance in F cm^{-2}, $\int idV$ the integrated area of the CV curve, S the surface area of active materials in the single electrode in cm^2 and it is fixed at 1 cm^2 in this study, ΔV the scanning potential window in V and v the scan rate in V s^{-1}.

Fig. 5b exhibits the dependence of the areal capacitance on varying CV scan rates of two types of electrodes, the PEDOT/SDS-GO electrodes display the areal capacitance of 79.6 mF cm^{-2} at 10 mV s^{-1}, which is larger than 73.3 mF cm^{-2} at 10 mV s^{-1} exhibited by the PEDOT/SDS electrodes, and it is higher than that of PANI/graphite oxide composites (25 mF cm^{-2} at 5 mV s^{-1}) and TiO_2@PPy core–shell nanowires electrode (64.6 mF cm^{-2} at 10 mV s^{-1}) reported previously [45,48]. Moreover, compared to the PEDOT/SDS electrodes, the PEDOT/SDS-GO electrodes show the larger areal capacitance value at all other scan rates. The CV test results indicate the incorporation of GO into the composites can effectively boost the capacitive performance in PEDOT-based supercapacitors.

Fig. 5c shows the GCD curves of PEDOT/SDS and PEDOT/SDS-GO electrodes at the current density rang form 0.1–5 mA cm^{-2}. It can be seen from the 0.1 mA cm^{-2} plots that both types of electrodes exhibit triangular-shape charge/discharge curves, but PEDOT/SDS-GO electrodes have the longer discharge time than that of PEDOT/SDS electrodes. Furthermore, the columbic efficiency (η) can be determined by calculating the ratio of discharge time t_d to charge time t_c according to the GCD curves. The calculated results manifest the η of PEDOT/SDS-GO electrodes is 98.5%, which is higher than 96.5% of PEDOT/SDS electrodes. The higher current density GCD curves range from 1 to 5 mA cm^{-2} also exhibit the same results that PEDOT/SDS-GO electrodes have the longer discharge time. Meanwhile, the PEDOT/SDS-GO electrodes also show the lower iR drops at all GCD current densities. As a result of the iR drop is usually caused by the overall internal resistance of the devices [30], the capacitor cells constructed with PEDOT/SDS-GO electrodes have the lower internal resistance. It should be pointed out that low internal resistance is of great importance in energy-storing devices as less energy will be wasted to produce unwanted heat during charging/discharging processes [49]. Based on the GCD curves measured by chronopotentiometry, the areal capacitance (C_S) value of a single electrode can be evaluated using the following Equation (2):

$$C_S = (2 \times i \times t)/(S \times \Delta V) \quad (2)$$

where C_s is the areal capacitance in F cm^{-2}, i the discharge current in A, t the discharge time in s, S the surface area of the active materials on the single electrode in cm^2 and ΔV the scan potential window in V.

Fig. 5d compares the areal capacitance value of two types of electrodes, the PEDOT/SDS-GO electrodes display the areal capacitance of 90.2 mF cm^{-2} at 0.1 mA cm^{-2}, while the PEDOT/SDS electrodes exhibit 84.2 mF cm^{-2} at 0.1 mA cm^{-2}, and the PEDOT/SDS-GO electrodes show the larger areal capacitance value at all varying GCD current densities, which is in accordance with the CV results. In addition, we can also observe from Fig. 5d that the gaps of areal capacitance value for two types of electrodes become bigger with the increase of GCD current densities, demonstrating the PEDOT/SDS-GO electrodes possess the better rate capability. Likewise, the GCD tests also indicate the as-prepared PEDOT/SDS-GO intercalation composites by incorporating GO into the composites improve the capacitive performance of electrodes. In addition, according to the morphology characterization above, the surface of GO became fluffy because of the incorporation of PEDOT coatings and PEDOT/SDS particles and formed layer-on/within-layer composite structure. Such a special microstructure might have led to more sites that were susceptible to redox reactions, a greater active area, and consequently, higher capacitance.

To further confirm the superiority of the PEDOT/SDS-GO composites over the PEDOT/SDS applied for supercapacitor electrodes, the EIS tests were made and the resulting Nyquist plots at open-circuit potentials are illustrated in Fig. 6a. The impedance plots of two types of electrodes are featured by a vertical trend at low frequencies, indicating capacitive behavior according to the equivalent circuit theory [50], and the straight line in the low frequency for PEDOT/SDS-GO electrodes lean more towards imaginary axis, manifesting that they have better capacitive character. In addition, a semicircle at high frequency is not detected for the two types of electrodes, which is attributed to the low interfacial charge-transfer resistance because of their high conductivity of films [37]. Another important information can be obtained from the plots at higher frequencies is the knee frequency, beyond which the capacitive behavior is replaced by the more inclined diffusion line, and the higher knee frequency means the lower diffusion impedance and faster charge transfer rates [50]. It can be found from the inset of Fig. 6 that PEDOT/SDS-GO electrodes have the higher knee frequency, this will be favorable for the rapid charge/discharge performance, as the results exhibited in the CV and GCD tests. Fig. 6b presents the conversion capacitance obtained from EIS. The areal capacitance values of single electrode can be calculated from the following Eq. (3) [51]:

$$C_S = -1 \Big/ \left(\pi S f Z''\right) \quad (3)$$

Thereinto, C_S is the areal capacitance in F cm^{-2}, f the frequency in Hz, Z'' the imaginary part of EIS in Ω, and S the geometric surface area of active materials on single electrode (1 cm^2 in this study). It can be seen from Fig. 6b that PEDOT/SDS-GO electrodes exhibit the higher areal capacitance at the whole frequency region compared with those of PEDOT/SDS electrodes, which is in good agreement with the results measured in CV and GCD tests.

3.4. Ragone plot and cyclic stability

Commonly, the areal energy and power density are used for evaluating thin film micro-batteries because the comparison has no dependence on the choice of other components including substrates and protective packaging [52]. The areal energy density and power density of the single electrode depicted in the Ragone plot can be calculated by using the Equations (4) and (5), respectively [45].

$$E = \frac{\frac{1}{2} C_S \Delta V^2}{3600} \quad (4)$$

$$P = \frac{3600E}{t} \quad (5)$$

where E is the areal energy density in Wh cm^{-2}, P the areal power density in W cm^{-2}, C_S the areal capacitance in F cm^{-2}, ΔV the

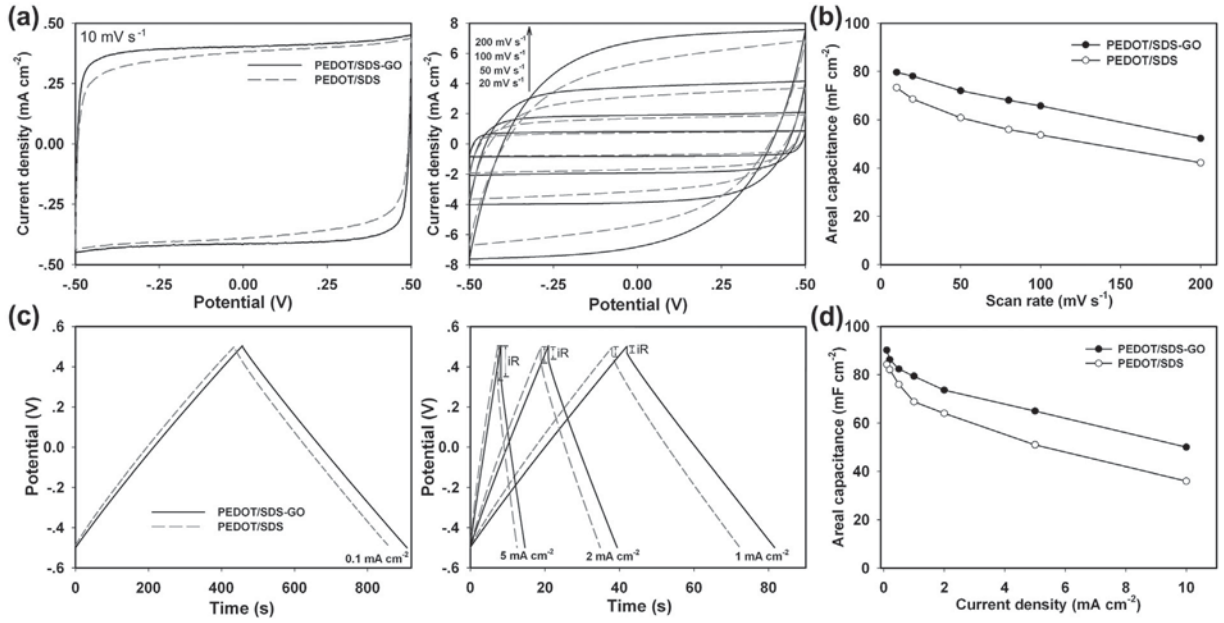

Fig. 5. (a) CV curves of the PEDOT/SDS and PEDOT/SDS-GO at different scan rates range from 10 mV s^{-1} to 200 mV s^{-1}; (b) Relationship of the areal capacitance with CV scan rate for PEDOT/SDS and PEDOT/SDS-GO composites; (c) GCD curves of the PEDOT/SDS and PEDOT/SDS-GO at different GCD current densities; (d) Areal capacitance *vs.* GCD current density for PEDOT/SDS and PEDOT/SDS-GO composites.

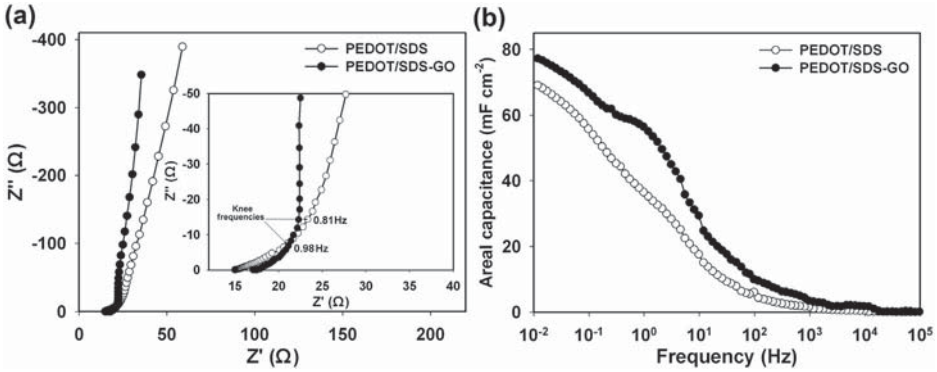

Fig. 6. (a) Nyquist plots of the supercapacitor cells assembled by PEDOT/SDS and PEDOT/SDS-GO electrodes, insert is the EIS in high-frequency region; (b) The relationship of areal capacitance with frequency for PEDOT/SDS and PEDOT/SDS-GO electrodes.

potential window (excluding *i*R drop in the beginning of the discharge) in V and *t* the discharge time in s.

A Ragone plot (Fig. 7a) is made according to the above formulas to compare the energy and power performance of PEDOT/SDS-GO and PEDOT/SDS electrodes. We can see the PEDOT/SDS-GO electrodes present the higher energy and power densities than those of PEDOT/SDS electrodes all the time. The PEDOT/SDS-GO electrodes show an energy density of 12.5 μWh cm^{-2} at a power density of 99.7 μW cm^{-2}, while it maintains 4.88 μWh cm^{-2} at 7027 μW cm^{-2}, presenting higher energy density and power density compared with previous reports on conducting polymers [45]. This high power capability may be attributed to the fast kinetic reaction of porous petal-like intercalated microstructures of PEDOT/SDS-GO composites permitting counter-ions which could diffuse into the polymer and provide a short diffusion distance to facilitate the ion transport.

The cycle life is a significant performance for the electrodes of supercapacitor, in this study, 5000 CV cycles at the scan rate of 100 mV s^{-1} were carried out to investigate the stability of the cells assembled by the test electrodes and the results are illustrated in Fig. 7b. We can observe that the cycle measurements for PEDOT/SDS-GO cause an increase in the capacitance up to 1000 cycles. It can be possibly related to a cycling measurement induced improvement in the surface wetting of the electrode [53,54], which is attributed to the large electrochemical surface area caused by the incorporated GO, leading to more available electroactive surface area with the cycles. Especially, the PEDOT/SDS-GO electrodes do not exhibit the decrease at the subsequent 4000 cycles, indicating the PEDOT/SDS-GO electrodes possess the excellent electrochemical stability. As the comparison, the capacitive retention rate of PEDOT/SDS electrodes decreases to 97.5% after 5000 CV cycles. The improved stability can be ascribed to the GO nanosheets provide a robust support for the CPs, thus enhances the mechanical strength of the composites and prevents the CPs from swelling and shrinking during the long-term cycling. Generally, the capacitive behavior and improved stability obtained for PEDOT/SDS-GO composites can be ascribed to the following three aspects: (1) The synergic effect of GO sheets and CPs; (2) The uniform coatings of CPs on GO sheets prevent them from aggregating, leading to improved electrical double-layer capacitance; (3) PEDOT/SDS particles and PEDOT-coated GO sheets form layer-on/within-layer petal-like composite structure. Therefore, the composite materials exhibit the better capacitive behavior and stability compared with those of the pristine polymers.

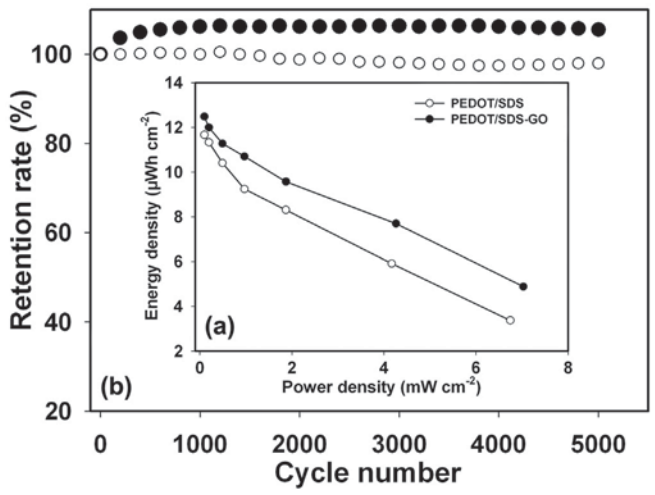

Fig. 7. (a) Ragone plots of PEDOT/SDS and PEDOT/SDS-GO electrodes; (b) The relationship of capacitance retention rate and cycle number for PEDOT/SDS (○)and PEDOT/SDS-GO (●) electrodes at 100 mV s^{-1} CV scan for 5000 cycles.

4. Conclusions

PEDOT/SDS-GO composite material is synthesized using an in situ electrochemical polymerization method in the presence of EDOT, GO, and SDS. The SEM, TEM, FT-IR, and XRD studies have shown the GO not only makes the composite material but also acts as a dopant to the PEDOT system, and the PEDOT/SDS-GO films show a special microstructure of petal-like intercalation composites. The electrochemical characterizations indicate the special intercalated microstructure with the contributions of both electrical double-layer capacitance and pseudocapacitance effectively boosts the electrochemical performance in PEDOT-based supercapacitor electrodes, and the PEDOT/SDS-GO composites exhibit a high areal capacitance of 79.6 mF cm^{-2} at 10 mV s^{-1} and maintain the original capacitance for 5000 CV cycles. This facile and one-step approach for the electrodes preparation of PEDOT/SDS-GO intercalation composites further extends the application of GO and should be very promising for the fabrication of low-cost, high-performance electrochemical supercapacitors for energy storage.

Acknowledgments

The authors appreciate funding from National Natural Science Foundation of China (21274082 and 21073115) and Shanxi Province (2012021021-3), the Program for New Century Excellent Talents in University (NCET-10-0926), and the Scientific Research Start-up Funds of Shanxi University (020351801002).

References

[1] M.R. Lukatskaya, O. Mashtalir, C.E. Ren, Y. Dall'Agnese, P. Rozier, P.L. Taberna, M. Naguib, P. Simon, M.W. Barsoum, Y. Gogotsi, Science 341 (2013) 1502–1505.
[2] D. Yu, K. Goh, H. Wang, L. Wei, W. Jiang, Q. Zhang, L. Dai, Y. Chen, Nat. Nanotechnol. 9 (2014) 555–562.
[3] L. Kou, T. Huang, B. Zheng, Y. Han, X. Zhao, K. Gopalsamy, H. Sun, C. Gao, Nat. Commun. 5 (2014) 3754.
[4] S. Chabi, C. Peng, D. Hu, Y.Q. Zhu, Adv. Mater. 26 (2014) 2440–2445.
[5] K. Wang, H.P. Wu, Y.N. Meng, Z.X. Wei, Small 10 (2014) 14–31.
[6] X. Lu, M. Yu, G. Wang, Y. Tong, Y. Li, Energy Environ. Sci. 7 (2014) 2160–2181.
[7] Y.W. Zhu, S. Murali, M.D. Stoller, K.J. Ganesh, W.W. Cai, P.J. Ferreira, A. Pirkle, R.M. Wallace, K.A. Cychosz, M. Thommes, D. Su, E.A. Stach, R.S. Ruoff, Science 332 (2011) 1537–1541.
[8] L.J. Deng, J.F. Wang, G. Zhu, L.P. Kang, Z.P. Hao, Z.B. Lei, Z.P. Yang, Z.H. Liu, J. Power Sources 248 (2014) 407–415.
[9] L. Zhang, X. Yang, F. Zhang, G.K. Long, T.F. Zhang, K. Leng, Y.W. Zhang, Y. Huang, Y.F. Ma, M.T. Zhang, Y.S. Chen, J. Am. Chem. Soc. 135 (2013) 5921–5929.
[10] X. Lu, Y. Zeng, M. Yu, T. Zhai, C. Liang, S. Xie, M.S. Balogun, Y. Tong, Adv. Mater. 26 (2014) 3148–3155.
[11] J. Yang, S. Gunasekaran, Carbon 51 (2013) 36–44.
[12] M.G. Jeong, K. Zhuo, S. Cherevko, W.J. Kim, C.H. Chung, J. Power Sources 244 (2013) 806–811.
[13] J.T. Zhang, X.S. Zhao, Chemsuschem 5 (2012) 818–841.
[14] M.J. Zhi, C.C. Xiang, J.T. Li, M. Li, N.Q. Wu, Nanoscale 5 (2013) 72–88.
[15] Y.T. Weng, N.L. Wu, J. Power Sources 238 (2013) 69–73.
[16] J.T. Zhang, X.S. Zhao, J. Phys. Chem. C 116 (2012) 5420–5426.
[17] T. Lindfors, R.M. Latonen, Carbon 69 (2014) 122–131.
[18] H.L. Cao, X.F. Zhou, Y.M. Zhang, L. Chen, Z.P. Liu, J. Power Sources 243 (2013) 715–720.
[19] C.C. Xiang, M. Li, M.J. Zhi, A. Manivannan, N.Q. Wu, J. Power Sources 226 (2013) 65–70.
[20] T. Zhai, F.X. Wang, M.H. Yu, S.L. Xie, C.L. Liang, C. Li, F.M. Xiao, R.H. Tang, Q.X. Wu, X.H. Lu, Y.X. Tong, Nanoscale 5 (2013) 6790–6796.
[21] C.L. Liang, T. Zhai, W. Wang, J. Chen, W.X. Zhao, X.H. Lu, Y.X. Tong, J. Mater. Chem. A 2 (2014) 7214–7220.
[22] C.H. Lei, P. Wilson, C. Lekakou, J. Power Sources 196 (2011) 7823–7827.
[23] D.R. Dreyer, S. Park, C.W. Bielawski, R.S. Ruoff, Chem. Soc. Rev. 39 (2010) 228–240.
[24] Z.F. Li, H.Y. Zhang, Q. Liu, Y.D. Liu, L. Stanciu, J. Xie, Carbon 71 (2014) 257–267.
[25] A.R. Liu, C. Li, H. Bai, G.Q. Shi, J. Phys. Chem. C 114 (2010) 22783–22789.
[26] J. Li, H.Q. Xie, Y. Li, J. Power Sources 241 (2013) 388–395.
[27] S. Sahoo, S. Dhibar, G. Hatui, P. Bhattacharya, C.K. Das, Polymer 54 (2013) 1033–1042.
[28] H.H. Chang, C.K. Chang, Y.C. Tsai, C.S. Liao, Carbon 50 (2012) 2331–2336.
[29] T. Lindfors, A. Osterholm, J. Kauppila, M. Pesonen, Electrochim. Acta 110 (2013) 428–436.
[30] H. Zhou, G. Han, Y. Xiao, Y. Chang, H.-J. Zhai, J. Power Sources 263 (2014) 259–267.
[31] A. Osterholm, T. Lindfors, J. Kauppila, P. Damlin, C. Kvarnstrom, Electrochim. Acta 83 (2012) 463–470.
[32] N. Sakmeche, S. Aeiyach, J.J. Aaron, M. Jouini, J.C. Lacroix, P.C. Lacaze, Langmuir 15 (1999) 2566–2574.
[33] Y.X. Xu, H. Bai, G.W. Lu, C. Li, G.Q. Shi, J. Am. Chem. Soc. 130 (2008) 5856.
[34] Y.Z. Chang, G.Y. Han, M.Y. Li, F. Gao, Carbon 49 (2011) 5158–5165.
[35] J.C. Meyer, A.K. Geim, M.I. Katsnelson, K.S. Novoselov, D. Obergfell, S. Roth, C. Girit, A. Zettl, Solid State Commun. 143 (2007) 101–109.
[36] C.Z. Zhu, J.F. Zhai, D. Wen, S.J. Dong, J. Mater. Chem. 22 (2012) 6300–6306.
[37] Y.Q. Han, B. Ding, H. Tong, X.G. Zhang, J. Appl. Polym. Sci. 121 (2011) 892–898.
[38] H.J. Shin, S.S. Jeon, S.S. Im, Synth. Met. 161 (2011) 1284–1288.
[39] D. Han, G. Yang, J. Song, L. Niu, A. Ivaska, J. Electroanal. Chem. 602 (2007) 24–28.
[40] L. Chen, C.Z. Yuan, H. Dou, B. Gao, S.Y. Chen, X.G. Zhang, Electrochim. Acta 54 (2009) 2335–2341.
[41] H.L. Guo, X.F. Wang, Q.Y. Qian, F.B. Wang, X.H. Xia, ACS Nano 3 (2009) 2653–2659.
[42] Y.Z. Chang, G.Y. Han, J.P. Yuan, D.Y. Fu, F.F. Liu, S.D.A. Li, J. Power Sources 238 (2013) 492–500.
[43] F. Alvi, M.K. Ram, P.A. Basnayaka, E. Stefanakos, Y. Goswami, A. Kumar, Electrochim. Acta 56 (2011) 9406–9412.
[44] K.V.,E. Frackowiak, F. Beguin, Electrochim. Acta 50 (2005) 2499–2506.
[45] H.G. Wei, J.H. Zhu, S.J. Wu, S.Y. Wei, Z.H. Guo, Polymer 54 (2013) 1820–1831.
[46] Y.Y. Horng, Y.C. Lu, Y.K. Hsu, C.C. Chen, L.C. Chen, K.H. Chen, J. Power Sources 195 (2010) 4418–4422.
[47] J.P. Liu, J. Jiang, M. Bosman, H.J. Fan, J. Mater. Chem. 22 (2012) 2419–2426.
[48] M.H. Yu, Y.X. Zeng, C. Zhang, X.H. Lu, C.H. Zeng, C.Z. Yao, Y.Y. Yang, Y.X. Tong, Nanoscale 5 (2013) 10806–10810.
[49] M. Jin, Y.Y. Liu, Y.L. Li, Y.Z. Chang, D.Y. Fu, H. Zhao, G.Y. Han, J. Appl. Polym. Sci. 122 (2011) 3415–3422.
[50] C. Peng, J. Jin, G.Z. Chen, Electrochim. Acta 53 (2007) 525–537.
[51] K.S. Ryu, Y.G. Lee, K.M. Kim, Y.J. Park, Y.S. Hong, X.L. Wu, M.G. Kang, N.G. Park, R.Y. Song, J.M. Ko, Synth. Met. 153 (2005) 89–92.
[52] N.J. Dudney, Electrochem. Soc. Interface 17 (2008) 44.
[53] Y.F. Xu, I. Hennig, D. Freyberg, A.J. Strudwick, M.G. Schwab, T. Weitz, K.C.P. Cha, J. Power Sources 248 (2014) 483–488.
[54] H.L. Wang, C.M.B. Holt, Z. Li, X.H. Tan, B.S. Amirkhiz, Z.W. Xu, B.C. Olsen, T. Stephenson, D. Mitlin, Nano Res. 5 (2012) 605–617.